Glycerol Selective Oxidation to Lactic Acid over AuPt Nanoparticles; Enhancing Reaction Selectivity and Understanding by Support Modification

Mark Douthwaite,[a] Natasha Powell,[a] Aoife Taylor,[a] Grayson Ford,[a] José Manuel López,[b] Benjamin Solsona,[c] Nating Yang,[a] Olga Sanahuja-Parejo,[b] Qian He,[a] David J. Morgan,[a] Tomas Garcia,*[b] and Stuart H. Taylor*[a]

A high surface area mesoporous TiO_2 material (110 m^2/g) was synthesised using a nanocasting methodology, utilizing SBA-15 as a hard template. This material was subsequently used as a support to prepare a series of 1 wt.% AuPt/TiO_2 catalysts, synthesised by conventional impregnation and sol-immobilisation. Catalysts were tested for the oxidation of glycerol to lactic acid and their performance was compared with corresponding catalysts supported on TiO_2–P25, TiO_2-anatase and TiO_2-rutile. Higher rates of reaction and higher selectivity to lactic acid were observed over nanocast TiO_2 supported catalysts. The increased performance of these catalysts was attributed to the presence of Si on the surface of the support, which likely arose from inefficient etching of the SBA-15 template. The presence of Si in these catalysts was confirmed by X-ray photoelectron spectroscopy and electron energy loss spectroscopy. It was proposed that the residual Si present increases the Brønsted acidity of the TiO_2 support, which can lead to the formation of Lewis acid sites under reaction conditions; both sites are known to catalyse the dehydration of a primary alcohol in glycerol. Typically, under alkaline conditions, lactic acid is formed by the nucleophilic abstraction of a hydrogen. Thus, we propose that the improved selectivity to lactic acid over the nanocast TiO_2 supported catalyst is attributed to the co-operation of heterogeneous and homogeneous dehydration reactions, as both compete directly with a direct oxidation pathway, which leads to the formation of oxidation products such as glyceric and tartronic acid.

Introduction

The efficient valorisation of glycerol to high-value products is of interest to both academics and industrialists.[1,2] Glycerol is a major by-product formed in the production of first generation biofuels; an industry which is projected to grow in the coming years and is driven by the demand for alternative and sustainable routes to liquid fuels and chemical feedstocks. Indeed, the highly functionalised nature of glycerol means that numerous different strategies can be employed for its up grading. For liquid phase valorisation, some of the most notable developments have utilized heterogeneous catalysis for the hydrogenolysis[3,4] or oxidation of glycerol,[5] both of which have displayed promising potential to date.

The selective aerobic oxidation of glycerol over supported Au containing catalysts has been widely investigated over the past 20 years.[6] Glycerol is an ideal model substrate to investigate the physicochemical properties of such catalysts due to its highly functionalised nature. Much of the early work investigating supported Au catalysts for liquid phase oxidation reactions was conducted by Prati, Rossi and co-workers.[7,8] Subsequently, many reports have been published investigating the use of mono-, bi- and even tri-metallic supported catalysts,[9–12] which has led to a greater understanding of properties that drive the selectivity in this reaction. In addition, contributions from Davis and co-workers supplemented this understanding by conducting a series of experiments, which elegantly confirmed the roles of H_2O, ^{-}OH and O_2 in this reaction over Au nanoparticles.[13] To date, it is widely acknowledged that reaction selectivity in this system can be controlled by a number of differing catalytic properties, including: the noble metal(s) particle size[14] and the properties of the support.[15]

Initially, emphasis was placed on the design and synthesis of heterogeneous catalysts, which could selectively oxidise

[a] Dr. M. Douthwaite, N. Powell, A. Taylor, G. Ford, Dr. N. Yang, Dr. Q. He, Dr. D. J. Morgan, Prof. S. H. Taylor
Cardiff Catalysis Institute
School of Chemistry
Cardiff University
Main Building
Park Place
Cardiff, CF10 3AT (UK)
E-mail: taylorsh@cardiff.ac.uk
[b] Dr. J. M. López, O. Sanahuja-Parejo, Dr. T. Garcia
Instituto de Carboquímica (ICB-CSIC)
C/Miguel Luesma Castán
50018 Zaragoza (Spain)
E-mail: tomas@icb.csic.es
[c] Dr. B. Solsona
Departament d'Enginyeria Química, ETSE
Universitat de València
Av. Universitat
46100 Burjassot, Valencia (Spain)

Supporting information for this article is available on the WWW under https://doi.org/10.1002/cctc.202000026

© 2020 The Authors. Published by Wiley-VCH Verlag GmbH & Co. KGaA. This is an open access article under the terms of the Creative Commons Attribution License, which permits use, distribution and reproduction in any medium, provided the original work is properly cited.

 © 2020 The Authors. Published by Wiley-VCH Verlag GmbH & Co. KGaA

glycerol to glyceric (GLA) and tartronic acid (TA), avoiding any C–C cleavage, which have previously been associated with the formation of H_2O_2 during the reaction.[6,16,17] Recently however, much more attention has been given to the formation of lactic acid (LA) from glycerol.[18,19] LA has a number of different applications, perhaps the most notable is its use as a feedstock for the formation of polylactic acid. Many prominent strategies have been adopted for this transformation, which have been elegantly surveyed in a recent review by Belousov and co-workers.[18] > One such strategy involves the use of supported noble metal catalysts under alkaline conditions,[20–23] typically leading to the formation of the corresponding lactate salt. It is important to note that any acid products formed in these reactions under alkaline conditions will likely exist as the conjugate salt.

Given the abundance of research in this area, there is a very good understanding of how each of the products are formed; see Scheme 1. Glycerol first undergoes an oxidative dehydrogenation reaction to produce either glyceraldehyde (GLD) or dihydroxyacetone (DHA). Under alkaline conditions, these substrates are rarely observed, indicating that they are rapidly consumed in a sequential reaction. The GLD and DHA formed subsequently either undergo a sequential oxidation to produce GLA, or dehydration to produce pyruvaldehyde (PALD). Given that these two pathways are considered to be in competition, it is somewhat unsurprising that higher yields of LA are typically observed when the temperature and the pH of the aqueous solution are increased.[22]

In addition to the reaction conditions, the physicochemical properties of the catalyst can have a significant effect on the selectivity of each reaction pathway.[5,6,15] Recent work by Evans *et al.*[24] revealed how influential the support material was for directing the reaction selectivity under basic conditions. It was determined that the oxygen adsorption capacity of La containing perovskite supports for AuPt nanoparticles had a significant influence on the reaction selectivity. Alloyed supported AuPt nanoparticles have emerged as promising catalyst for the aerobic oxidation of glycerol to LA under alkaline conditions. The high performance of these catalysts has been attributed to synergistic interactions between the two metals. The incorporation of Pt is considered to assist with the base catalysed dehydration of the reaction intermediate, and also improves catalyst stability.[23]

Alternative strategies have also been developed for the synthesis of LA from glycerol under base-free conditions. Under such conditions, a strong Bronsted acidic material is typically

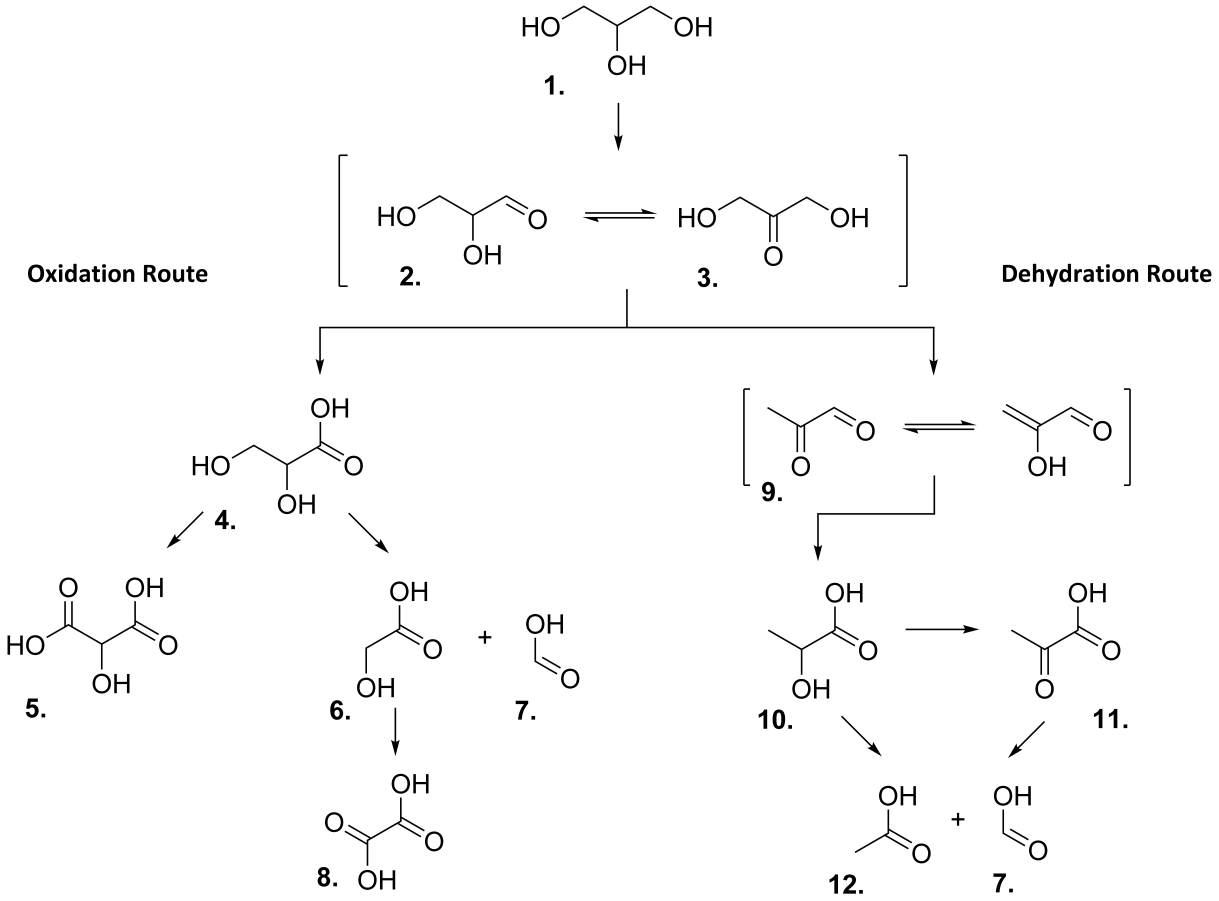

Scheme 1. Reaction scheme for the liquid phase aerobic oxidation of glycerol over noble metal supported catalysts. **Key:** 1. Glycerol; 2. Glyceraldehyde; 3. Dihydroxyacetone; 4. Glyceric acid; 5. Tartronic acid; 6. Glycolic acid; 7. Formic acid; 8. Oxalic acid; 9. Pyruvaldehyde; 10. Lactic acid; 11. Pyruvic acid; 12. Acetic acid.

© 2020 The Authors. Published by Wiley-VCH Verlag GmbH & Co. KGaA

employed as either a support or as a co-catalyst.[18] In the absence of base, this material serves as a catalyst for both the dehydration of GLD and intramolecular rearrangement of PALD to LA. Subsequent work has evidenced that Lewis acidity is affective at catalysing both the dehydration and rearrangement reactions.[25–27] While this approach is undeniably more desirable from an industrial perspective, it too has limitations. Perhaps the most pertinent of these is the substantially lower rates of reaction which are commonly observed under base-free conditions. This is because the $^{-}$OH plays a crucial role in the activation of the C–H bond, widely accepted to be the rate determining step in the oxidation of glycerol over supported heterogeneous catalysts.[13] A number of studies have shown that improved rates of reaction can be achieved by increasing the reaction temperature and partial pressure of O_2.[28,29] Heeres and co-workers subsequently developed this further;[30] in the presence of methanol and a Lewis acidic co-catalyst, the authors demonstrated that appreciable yields of methyl lactate could be produced from glycerol.

In this study, we investigate how the use of a nanocast TiO_2 support can influence the reaction selectivity of AuPt nanoparticles in the aerobic oxidation of glycerol to LA under comparatively mild, alkaline conditions. Herein, we demonstrate that the application of a nanocast mesoporous TiO_2 support for AuPt nanoparticles can result in a higher reaction selectivity to LA during the oxidation of glycerol, when compared to a corresponding AuPt/TiO_2-catalyst prepared using conventional titania.

Experimental

Chemicals, Source and Purity

Acetic acid (Sigma-Aldrich, ≥99.7%); Acetone (Scharlau, analytical grade); Chloroauric acid (Strem, 99.8%); Chloroplatinic acid hexahydrate (Sigma Aldrich, ACS reagent, 37.5% Pt basis); Formic acid (Sigma Aldrich, ≥98%); Glyceric acid (TCI, 40% in water); Glycerol (Sigma-Aldrich, ≥99.5%); Glycolic acid (Sigma-Aldrich, 99%); Hydrochloric acid (Scharlau, 37% reagent grade); DL-Lactic Acid (Sigma-Aldrich, 85%); Oxalic acid (Sigma-Aldrich, ≥99.99%); Phosphoric Acid (Sigma-Aldrich, (85 wt.% in H_2O) ≥99.99%); Pluronic P123 (Mw = 5800, EO20PO70EO20) (Sigma-Aldrich); Polyvinylalcohol (Sigma-Aldrich, 80% Hydrolysed); Sodium Borohydride (Sigma-Aldrich, 99.99%); Sodium Hydroxide (Fischer Scientific, 99.3%); Tartronic acid (Sigma-Aldrich, ≥97%); Tetraethoxysilane (TEOS) (Sigma-Aldrich, >99%); Titania, Anatase (Sigma-Aldrich, 99.7%); Titainia P.25 (Degussa, ≥99.5%,); Titainia, Rutile (Sigma-Aldrich, 99.995%); Titanium(IV) isopropoxide (Sigma-Aldrich, 97%); Water, (Fisher Scientific, HPLC grade).

Catalyst Synthesis

Nanocast TiO_2 (TiO_2–NC) was synthesised using a hard-templating methodology. First, ordered mesoporous silica SBA-15 template with a rod-like morphology was prepared according to the synthetic process reported in the literature.[31] In a typical synthesis, P123 (2 g) was dissolved in HCl (75 mL, 2 M) solution with stirring, followed by addition of TEOS (4 mL) to the homogeneous solution. This gel was stirred at 40 °C for 24 h, and then crystallized at 100 °C for 24 h under static conditions. The resulting solid was filtered, washed, dried for 16 h at 100 °C and calcined at 550 °C in air for 6 h. Secondly, ordered mesoporous TiO_2 was synthesized using the hard template method reported previously.[32] In a typical preparation, titanium(IV) isopropoxide (12 mmol) was dissolved in acetone (15 mL). After the solution became clear, SBA-15 hard template (2 g) was added and the mixture was stirred for 2 h, the solvent was then evaporated. In order to achieve higher loadings, the above dried powder was calcined at 200 °C for 6 h with a heating ramp rate of 1 °C min^{-1} to decompose the metal precursor, and then the impregnation step was repeated, but the amount of titanium(IV) isopropoxide was reduced to 8 mmol. The resulting sample was calcined in air at 500 °C for 4 h with the same heating ramp rate to completely decompose the inorganic precursor. Finally, the silica template was removed using a NaOH (2 M, 20 mL/g_{cat}) aqueous solution at 70 °C. In some cases, three additional washing steps were conducted on the TiO_2–NC material; abbreviated in the text as TiO_2–NC–W.

Au and Pt NP's were deposited onto the surface of the TiO_2 supports by conventional impregnation (IMP) and sol-immobilisation (SI) methods. For preparation by impregnation, $HAuCl_4$ (0.205 mL, 12.25 g/L) and H_2PtCl_6 (0.513 mL, 4.85 g/L) were added to a small beaker containing H_2O (0.782 mL). With stirring, the TiO_2 support (0.495 g) was subsequently added to the beaker and the solution was heated to 80 °C. The solution was carefully monitored and removed from the heat when the consistency of the mixture resembled that of a thick paste. The paste was then dried for 16 h at 110 °C. The catalyst was then calcined at 200 °C (ramp rate = 2 °C/min) in a tubular furnace under flowing air (50 mL/min) for 4 h.

For preparation by sol-immobilisation; $HAuCl_4$ (0.205 mL, 12.25 g/L) and H_2PtCl_6 (0.513 mL, 4.85 g/L) were added to a beaker containing H_2O (200 mL). PVA (0.325 mL, from 0.1 g PVA in 10 mL H_2O 80% hydrolysed) was then added and left to stir for 20 minutes. $NaBH_4$ (1.964 mL) was added to reduce the metals and stirred for 30 minutes. TiO_2 (0.495 g) was subsequently added and then acidified to pH 2 with drop-wise addition of concentrated H_2SO_4 and stirred for an additional 1 h. The resulting solution was then filtered under vacuum and washed with distilled water (500 mL), before the residue was dried for 16 h at 110 °C.

Catalyst Characterisation

BET analysis was conducted on a Quantachrome Quadrosorb instrument; the samples were first degassed at 200 °C for 4 h. Once degassed, 25 point nitrogen adsorption isotherms were collected at −196 °C, and data analysed using the BET method.

Powder X-ray diffraction (XRD) was acquired using a PANalytical X'Pert Pro system with a Cu Kα X-ray source operated at 40 kV and 40 mA. An X'Celerator detector was used with data collected from $2\theta = 10°$ to 80° for 30 minutes collection time.

X-ray Photoelectron Spectroscopy (XPS) measurements were performed using a Kratos Axis Ultra DLD instrument using a monochromatic Al Kα source ($h\nu = 1486.6$ eV) operating at 140 W (14 kV and 10 mA). Charge neutralisation was achieved using the Kratos immersion lens system and calibration of binding energies was conducted against the C1s line for adventitious carbon, taken to be 284.8 eV. High-resolution and survey scans were performed at energies of 20 and 160 eV respectively. Data were analysed using CasaXPS (v2.3.23) using modified Wagner sensitivity factors, as supplied by the manufacturer.

Ammonia temperature programmed desorption (NH_3–TPD) experiments were conducted on a Quantachrome ChemBET Chemisorption analyser equipped with a TCD. The titanium supports (100 mg) were first heated to 130 °C (15 °C/min) under He (30 mL/min) and

© 2020 The Authors. Published by Wiley-VCH Verlag GmbH & Co. KGaA

held at temperature for 1 h. After cooling to 30 °C, the sample(s) were exposed to NH_3 for 0.5 h at a flow rate of 30 mL/min, after which, the samples were heated to 1000 °C (10 °C/min) under He (30 mL/min).

Microscopy was performed using a Tescan Maia3 field emission gun scanning electron microscope (FEG-SEM) operating at 30 kV. Images were acquired using the secondary electron and backscattered electron detectors. Bright field scanning transmission electron images (STEM) were obtained using a STEM holder. Samples were dispersed as a powder onto 300 mesh copper grids coated with Holey carbon film. Transmission electron microscopy (TEM) was carried out using a JEOL JEM-2100 microscope with a LaB6 filament operating at 200 kV. Powdered catalyst samples were dry dispersed onto lacy carbon films over a 400 mesh copper grid. High angle annular dark field scanning transmission electron microscopy (HAADF-STEM) data were acquired using a JEOL ARM200CF microscope in the electron Physical Science Imaging Centre in Diamond. The instrument was operated at 200 kV and the electron energy loss spectroscopy was carried out using a Gatan Quantum Dual EELS spectrometer. Particle size distributions were calculated from the analysis of 100 particles for a given catalyst, using ImageJ. Fourier Transform Diffuse Reflectance Infrared (DRIFT) spectroscopic analysis of these TiO_2-based catalysts was performed on a VERTEX 70 Bruker spectrometer using a reaction chamber. Pyridine was used as a probe molecule for the qualitative and quantitative determination of the acidity of these materials. For these experiments, each catalyst was first heat-treated at 450 °C for 1 h in an N_2 stream to remove any physisorbed compound. Subsequently, the samples were cooled to 50 °C and pyridine vapour was introduced to the cell for 1 hour. The physically adsorbed pyridine was removed by flushing N_2 for 1 h. The sample was heated under a N_2 flow to different desorption temperatures (50, 100, 200, 300 and 400 °C). Spectra were collected for each material at these temperatures in the range of 2000–1350 cm^{-1} with a resolution of 4 cm^{-1}, obtained by averaging of 128 scans.

Quantification was performed in the 1600–1400 cm^{-1} range using the following equations:[33]

$$C_B = \frac{A_B \pi D^2}{4m\varepsilon_B} \quad (1)$$

$$C_L = \frac{A_L \pi D^2}{4m\varepsilon_L} \quad (2)$$

where A_B and A_L are the integrated zone of 1540 and 1450 cm^{-1} for the Brønsted and Lewis sites respectively. ε_B and ε_L are the molar extinction coefficients at those wavelengths taken from the literature, which are respectively 1.67 and 2.22 cm/μmol. D is the diameter of the powder in the reaction chamber and m is the mass of the sample used.

Catalyst Testing

A 50 mL Colaver glass reactor was placed in a heated oil bath containing a stirrer bar (110 °C, 800 RPM) and allowed to equilibrate for 30 minutes. To this, catalyst (substrate: AuPt molar ratio = 4055:1), NaOH (10 mL, 2.4 M), glycerol (10 mL, 0.6 M) and a magnetic stirrer was added to the reactor, before it was sealed, purged 5 times and charged with O_2 (3 bar). The reaction was stirred for the desired time (0.5–7.5 h) at 800 rpm. Once the reaction was complete, the reactor vessel was placed in an ice bath to cool for 15 minutes before depressurising the reactor. Two 0.5 mL samples were subsequently withdrawn and diluted 10 fold in H_2O to quench the reaction, after which they were filtered and quantified using an Agilent HPLC system. HPLC analysis was carried out using refractive index and diode array detectors. Reactants and products were separated over a Metacarb 67H column at a temperature of 50 °C. An isocratic mobile phase (H_3PO_4, 0.1 % in H_2O) was used with the flow rate fixed at 0.8 mL/min. Products were identified and quantified using an external calibration method. Response factors were obtained by calibration against authentic standards.

Results and Discussion

As discussed previously, AuPt/TiO_2–P.25 catalysts have been demonstrated to be selective for the formation of LA from glycerol.[23] Given that the application of mesoporous support materials can have a significant impact on both selectivity and activity in liquid phase oxidation reactions,[34] it is important to establish whether the application of such materials as supports for noble metal catalysts provide a promotional benefit in this reaction. As such, SBA-15 was used as a hard template for the formation of mesoporous-TiO_2. TEM and N_2 sorption experiments were conducted to probe the structural properties of this material (Figure 1).

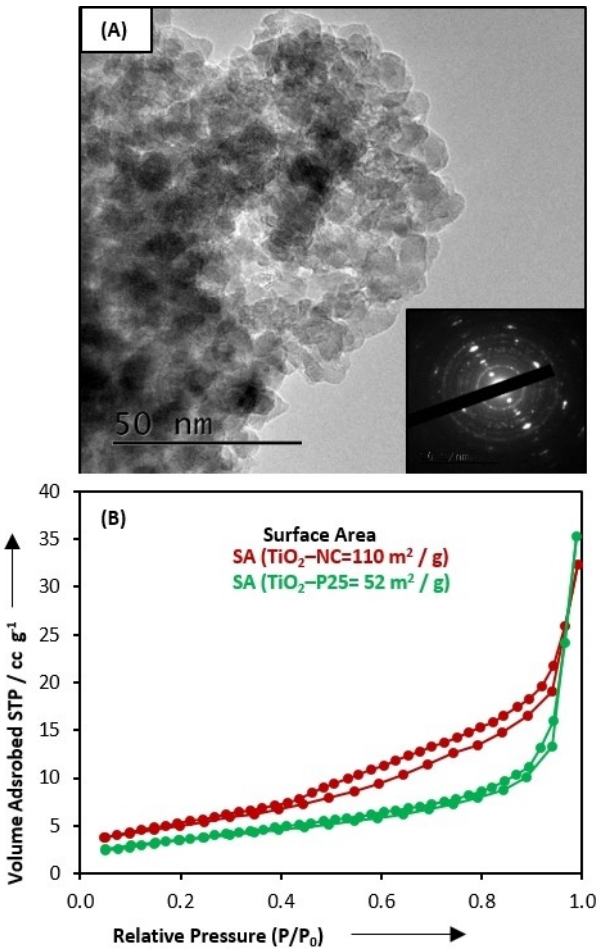

Figure 1. (A) TEM image and diffraction pattern of the TiO_2–NC material; (B) N_2 sorption isotherms and BET SA measurements for the TiO_2–NC (red) and TiO_2–P25 (green).

© 2020 The Authors. Published by Wiley-VCH Verlag GmbH & Co. KGaA

The TEM image displayed in Figure 1(A) confirmed that the nanocast TiO_2 (TiO_2–NC) did not exhibit a well-defined mesoporous structure, despite mesopores in SBA-15 being typically 3 to 7 nm in diameter. The material consisted of exceptionally small TiO_2 agglomerates; <30 nm in size. The perceived lack of an ordered mesoporous structure is likely to be a result of the interparticle mesoporosity created between the small TiO_2 crystallites. Despite this, evidence of mesoporosity can be deduced from the corresponding N_2 sorption isotherm (Figure 1 (B)). Whilst the isotherm does exhibit some type (IV) sorption character, it is poorly defined, albeit exhibiting a very different adsorption and desorption curve to that exhibited by TiO_2–P25, which is typically nanocrystalline in nature. The type (IV) character in the sorption isotherm of the TiO_2–NC support is evidence of mesoporosity, although TEM confirmed that the replication of the SBA-15 porous structure was not achieved.

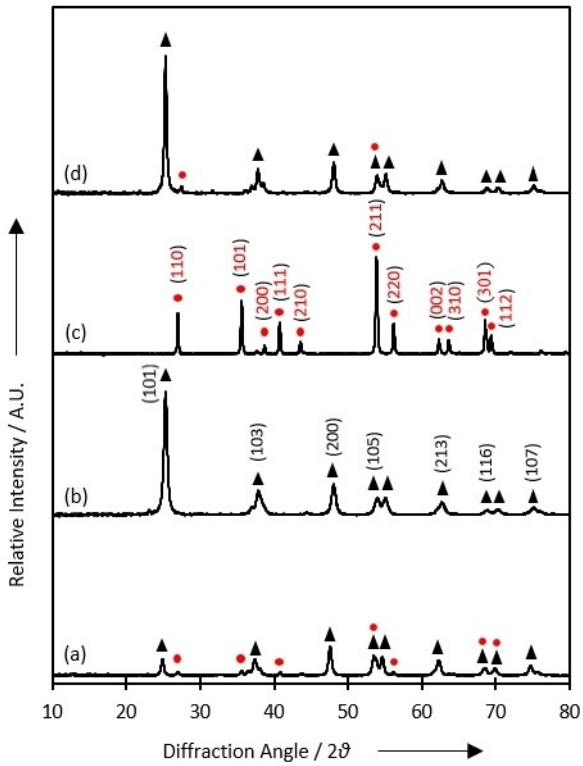

Figure 2. X-ray diffraction over the various TiO_2 support materials; (a) P25–TiO_2, (b) A–TiO_2, (c) R–TiO_2 and (d) NC–TiO_2. **Key:** Anatase (▲); Rutile (●).

TiO_2–P25 consists of both rutile and anatase phases with a ratio of approximately 1:3, respectively.[35] To establish whether the phase of the TiO_2 support material influenced the catalytic performance, two additional 1 wt.% AuPt catalysts, supported on TiO_2 anatase (TiO_2–A) and TiO_2 rutile (TiO_2–R) were prepared by impregnation. The structure of all four support materials were subsequently investigated by XRD and the corresponding diffraction patterns for each are displayed in Figure 2. The TiO_2–NC material predominantly consisted of anatase. However, a diffraction peak at *ca.* $2\theta = 27°$, which is characteristic of a rutile (110) reflection, confirmed that the NC–TiO_2 contained a small proportion of the rutile phase.

The surface area of all four supports was measured by BET, which confirmed that there were significant differences in the specific surface area of the materials (Table S1). The active metal dispersion in catalysts prepared by conventional impregnation can be dramatically affected by the total surface area of the support. Consequently, the dispersion of Au and Pt on each of the catalysts after impregnation was investigated by SEM (Figure S1). The particle size distribution (PSD) of metal particles on the surface of these materials differed significantly. The mean particle sizes for the AuPt/TiO_2–NC, AuPt/TiO_2–P25, AuPt/TiO_2–A and AuPt/TiO_2–R were determined to be 11.0, 49.3, 38.6 and 20.6 nm respectively (Table 1, Figure S1).

All four catalysts were subsequently tested for the aerobic oxidation of glycerol. The results from these experiments are displayed in Table 1. The reactions were conducted under previously optimised reaction conditions for LA production from glycerol over Pt/CeO_2 catalysts.[22] A highly alkaline medium (1.2 M) is required, as it promotes the dehydration pathway to LA; assisting with both the activation of the C–H and O–H bonds and promoting the intramolecular rearrangement of PALD. To ensure reactions were conducted under optimum conditions, the influence of reaction temperature on lactic acid selectivity was investigated (Table S2). The experiments confirmed that the optimum temperature for LA formation was 110 °C, which aligns with the findings of Heeres and co-workers,[22] who showed that increasing the reaction

Table 1. The aerobic oxidation of glycerol over a series of supported AuPt catalysts prepared by impregnation. The glycerol conversion (χ), product selectivity and CMB listed correspond to reactions run for 0.5 and 7 h over each of the catalysts.

Catalyst	Mean Particle Size [nm]	Time [h]	χ Glycerol [%]	Selectivity [%]								CMB [%]
				LA	GLA	TA	GLY	OXA	PA	AA	FA	
AuPt/TiO_2–P25	49.3	0.5	6	72	14	2	7	0	0	0	4	X
		7.0	82	61	15	5	12	0	0	0	6	103
AuPt/TiO_2–NC	11.0	0.5	10	84	11	1	3	0	0	0	2	X
		7.0	99	82	6	5	4	2	0	0	2	102
AuPt/TiO_2–A	38.6	0.5	3	38	22	2	24	0	0	0	14	X
		7.0	26	31	29	3	22	0	0	0	15	95
AuPt/TiO_2–R	20.6	0.5	9	76	8	1	10	0	0	0	5	X
		7.0	92	77	5	3	10	0	0	0	5	98

Reaction Conditions: Reaction solution (20 mL, 0.3 M glycerol, 1.2 M NaOH); 3 bar O_2; 110 °C; catalyst (0.029 g); time = stated. LA (lactic acid), GLA (glyceric acid), TA (tartronic acid), GLY (glycolic acid), OXA (oxalic acid), PA (pyruvic acid), AA (acetic acid); FA (formic acid); TiO_2–X; NC (nanocast), P25 (titania P25), A (anatase) and R (rutile).

© 2020 The Authors. Published by Wiley-VCH Verlag GmbH & Co. KGaA

temperature increased LA selectivity over a AuPt/CeO_2 catalyst. At temperatures in excess of 110 °C, LA is transformed to further oxidised products and is more susceptible to undergo C–C cleavage.

The AuPt/TiO_2–NC catalyst was the most active, exhibiting glycerol conversions of 10 and 99% after 0.5 and 7 h of reaction, respectively. Interestingly, the AuPt/TiO_2–NC material also exhibited a high reaction selectivity to LA (82%) at close to complete glycerol conversion. Relatively high reaction selectivity to LA was observed with the AuPt/TiO_2–R and AuPt/TiO_2–P25 catalysts; a LA selectivity of 77 and 61% were observed at glycerol conversions of 92 and 82%, respectively. The AuPt/TiO_2–A catalyst exhibited the lowest conversion and lowest selectivity to LA. It is therefore interesting that the AuPt/TiO_2–NC catalyst, which comprises predominantly of anatase, was selective to LA. For each reaction, the by-products were representative of those formed from the direct oxidation route (see Scheme 1). For each of the catalysts, no pyruvic acid (PA), or acetic acid (AA), was observed, indicating that it was unlikely that any LA was consumed through sequential reactions.

Given that the catalytic activity was so different after 7 h, it was important to investigate the reaction selectivity over each of the catalysts at low conversion. The same trend in catalytic activity was observed for the series of catalysts after 0.5 h and the highest reaction selectivity to LA was once again exhibited by the AuPt/TiO_2–NC catalyst. Indeed, the selectivity to LA over this catalyst at 0.5 h is remarkably similar to the LA selectivity observed at full conversion, indicating that there is no change in the rate of each reaction pathway over the duration of the reaction. For all the catalysts, the proportion of GLA to TA is higher at low conversion, which is unsurprising given that TA is a sequential oxidation product of GLA. Perhaps most interestingly, at *iso*-conversion the selectivity to LA over the AuPt/TiO_2–NC catalyst is appreciably higher than that observed even over the AuPt/TiO_2–R catalyst. The observation that the AuPt/TiO_2–NC catalyst is more selective to LA, albeit comprising almost entirely of anatase, is of great interest, given that the corresponding catalyst prepared on TiO_2–A exhibited such poor selectivity to LA. This indicates that the AuPt/TiO_2–NC catalyst possesses some other physicochemical property which favours the formation of LA.

The supported metal particle size is another parameter which can influence reaction selectivity in this reaction.[14] As metal nanoparticles reduce in size their electronic properties can change, influencing the binding energy of substrate to the active sites on the nanoparticle.[36] This in turn, can effect the activity and selectivity of a catalyst. It was therefore important to ensure that the observed differences in reaction selectivity were not merely attributed to a particle size effect, a parameter which is typically influenced by the total surface areas of the support materials. Given that the surface areas of these four supports differed quite substantially (Table S1), it was important that an alternative preparation method was used to provide a similar dispersion of the AuPt nanoparticles. For this reason, two additional catalysts were prepared by sol immobilisation; a technique commonly employed to prepare supported metal catalysts with well-defined and narrow particle size distributions. This technique relies on the use of a stabilising agent to control the size of colloidal AuPt particles which are formed during metal reduction; see the experimental section for further details. In this study, polyvinyl alcohol (PVA) was used as the stabilising agent, as it has been demonstrated to provide a good metal dispersion, regardless of the support.[37] Characterisation by FEG-SEM (Figure S2) confirmed that the particle size distribution of these catalysts was indeed more uniform; the mean particle sizes for the 1 wt.% AuPt/TiO_2–$P.25_{SI}$ and 1 wt.% AuPt/TiO_2–NC_{SI} were determined to be 4.4 and 3.4 nm in diameter, respectively. In order to establish how this change in particle size from impregnation to sol immobilisation influenced their catalytic properties, both were tested for the oxidation of glycerol under the same conditions used previously. The results from these experiments are displayed in Table 2. To ensure that any differences in catalytic performance were not attributed to slight variations in the catalyst metal loading, a known quantity of each catalyst was digested in aqua regia and the Au and Pt quantified by MP-AES. The Au and Pt metal loadings were all considered to be comparable (Table S3).

Close to full glycerol conversion was observed over both catalysts after 7 h of reaction. The reaction selectivity to LA over the AuPt/TiO_2–NC_{SI} catalyst remains higher than that observed over the corresponding catalyst supported on TiO_2–$P25_{SI}$; reaction selectivity to LA of 71 and 69% were observed over

Table 2. The aerobic oxidation of glycerol over a series of supported AuPt catalysts prepared by sol immobilisation. W corresponds to an additional pre-washing step conducted on the support material prior to immobilisation with Au and Pt. The glycerol conversion (χ), product selectivity and CMB listed correspond to reactions run for 0.5 and 7 h over each of the catalysts.

Catalyst	Mean Particle Size [nm]	Time [h]	χ Glycerol [%]	Selectivity [%]								CMB [%]
				LA	GLA	TA	GLY	OXA	PA	AA	FA	
AuPt/TiO_2–P25	4.4	0.5	18	66	25	1	5	0	0	0	4	x
		7.0	100	69	7	18	3	1	1	1	1	98
AuPt/TiO_2–P25–W	–	0.5	17	67	24	1	5	0	0	0	3	x
		7.0	100	69	5	15	6	2	1	2	2	96
AuPt/TiO_2–NC	3.4	0.5	18	68	25	0	4	0	0	0	4	x
		7.0	100	71	16	5	5	0	0	1	3	99
AuPt/TiO_2–NC–W	–	0.5	18	68	22	1	3	0	0	0	6	x
		7.0	100	66	2	18	2	2	1	2	8	98

Reaction Conditions: Reaction solution (20 mL, 0.3 M glycerol, 1.2 M NaOH); 3 bar O_2; 110 °C; catalyst (0.029 g); time = stated. LA (lactic acid), GLA (glyceric acid), TA (tartronic acid), GLY (glycolic acid), OXA (oxalic acid), PA (pyruvic acid), AA (acetic acid); FA (formic acid); TiO_2–X; NC (nanocast), W (support material exposed to an additional washing procedure with NaOH).

© 2020 The Authors. Published by Wiley-VCH Verlag GmbH & Co. KGaA

these two catalysts respectively. At low conversion (0.5 h of reaction), the activity of both catalysts appears to be comparable, but the selectivity to LA appears to be slightly higher over the AuPt/TiO_2–NC_{SI} catalyst. Given that higher reaction selectivity to LA is observed with the AuPt/TiO_2–NC catalysts prepared by impregnation and sol-immobilisation, compared to the corresponding AuPt/TiO_2–P25 catalysts, it is unlikely that the enhanced LA selectivity is solely attributed to a particle size effect. Therefore, additional characterisation of these materials was conducted so that the origin of the effect could be established.

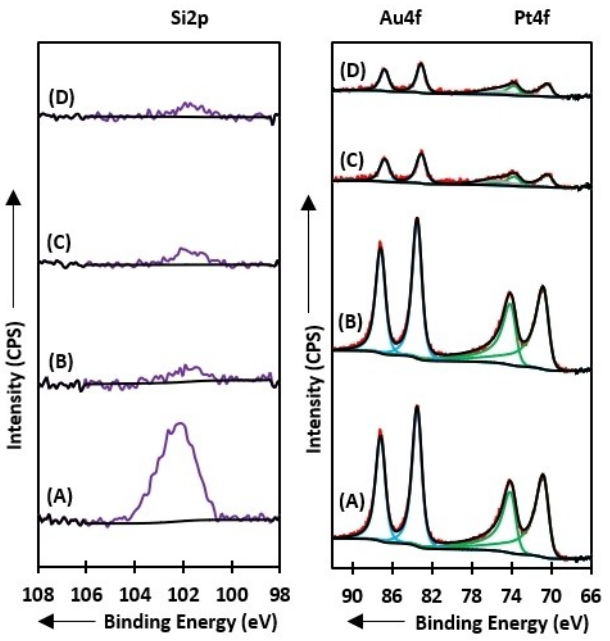

Figure 3. X-ray photoelectron spectroscopy data corresponding to Si2p, Au4f and Pt4f regions of different 1 wt.% AuPt/TiO_2 catalysts; (A) AuPt/NC–TiO_2, (B) AuPt/NC–TiO_2–W, (C) AuPt/P25–TiO_2 and (D) AuPt/P25–TiO_2–W. W corresponds to the additional washing of the support with NaOH (2 M), prior to immobilisation with AuPt nanoparticles.

Both catalysts were studied by XPS, the corresponding spectra are displayed in Figure 3. Fitting of Au4f and Pt4f regions confirmed that Au and Pt were present in the metallic state, which is unsurprising given the excess of reducing agent ($NaBH_4$) used in their preparation. Inspection of the Si2p region confirmed the presence of Si in the AuPt/TiO_2-NC_{SI} catalyst (Figure 3, Table S3), with a binding energy (BE) of 102.1 eV. Typically, Si^{4+} in the form of SiO_2 (*c.f.* SBA-15) is evidenced by a peak at a BE of *ca.* 103.5 eV. A lower BE, as observed here, is typically attributed to the loss of oxygen coordination of the Si centre and is attributed to residual SBA-15 or isolated regions of SiO_x. For lower concentrations of Si, the BE is observed to shift even lower (up to *ca.* 0.7 eV) but all other peaks remain within the limits of experimental uncertainty (*ca.* 0.2 eV). The presence of surface Si in the AuPt/TiO_2-NC catalyst was also evidenced by HAADF-EELS (Figure 4). The AuPt metal particles can be clearly visualized using the atomic number Z contrast high angle annular dark field (HAADF) imaging (Figure 4 (a–d)). Further evidence for the residual Si in the surface layer can be detected using electron energy loss spectroscopy (EELS). As

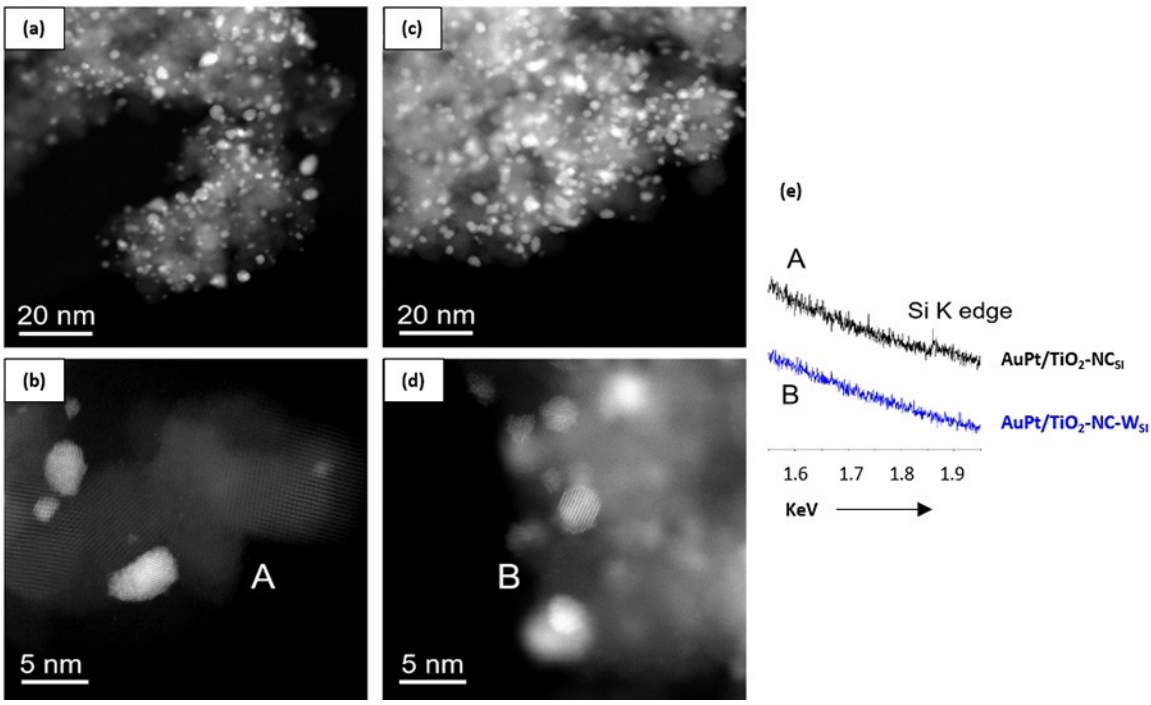

Figure 4. Relatively lower and higher magnification STEM-HAADF images of (a, b) AuPt/TiO_2 NC and (c,d) AuPt/TiO_2 NC W catalysts. (e) Electron energy loss spectroscopy (EELS) spectra, obtained by parking scanning a small area near the edge of the TiO_2 particle at locations labeled as A and B shown in images (c) and (d), respectively. A weak Si signal were identified on the AuPt/TiO_2–NCSI, but not on the AuPt/TiO_2–NC–WSI, which has undergone additional NaOH washing.

© 2020 The Authors. Published by Wiley-VCH Verlag GmbH & Co. KGaA

shown in Figure 4 (e). When scanning the near edge area of the nanocast TiO_2 particles, a week signal of Si K edge at *ca.* 1845 eV can be detected. However, for the AuPt/TiO_2-NC-W_{SI} catalyst, after additional washing by NaOH, this signal was no longer detected. Confirmation that traces of surface Si are present in this sample is unsurprising, as SBA-15 was used as a hard template in the production of the TiO_2-NC material, before being removed by dissolution. Evidently, the etching process does not result in total removal of the casting template leaving some Si embedded in the TiO_2 surface.

To determine whether the presence of surface Si in this catalyst was responsible for the higher selectivity to LA observed over the 1 wt.%AuPt/TiO_2–NC_{SI} catalyst, the TiO_2–NC material was subjected to three additional washing steps with NaOH (2 M), prior to immobilisation of Au and Pt nanoparticles (see experimental section for further details). This support was subsequently used to prepare an additional catalyst by SI; annotated to AuPt/TiO_2–NC–W_{SI}. This catalyst and a corresponding P25 supported control catalyst (AuPt/TiO_2–P25–W_{SI}) were also studied by XPS (Figure 3), and confirmed the additional washing step had removed a substantial quantity of the Si from the surface of the NC material (Figure 3, Table S4). Residual quantities of Si can be observed in the XPS spectra of the other three catalysts, but the proportion of Si in these three catalysts was comparable, and most likely originates from Si impurities in the samples. To establish what influence the surface Si exhibited on the catalytic performance, the washed catalysts were also investigated for the aerobic oxidation of glycerol (Table 2).

The removal of Si from the surface of the TiO_2–NC material clearly influenced the reaction selectivity. LA selectivity of 71 and 66% was observed for the AuPt/TiO_2–NC_{SI} and AuPt/TiO_2–NC–W_{SI} catalysts respectively, after 7 h of reaction. The reduction in selectivity to this pathway over the AuPt/TiO_2–NC_{SI} catalyst is further evidenced by evaluating the reaction selectivity toward TA and GLA at full conversion. For the AuPt/TiO_2–NC–W_{SI}, AuPt/TiO_2–$P25_{SI}$ and AuPt/TiO_2–P25–W_{SI} catalysts, a substantially higher selectivity to TA was observed, at the expense of GLA. This suggests that the AuPt/TiO_2–NC_{SI} catalyst is also not as effective for the sequential oxidation of GLA to TA. The comparable product distributions observed for the 7 h reactions over AuPt/TiO_2–$P25_{SI}$ and AuPt/TiO_2–P25–W_{SI} indicate that the differences between the NC and NC–W supported catalysts are not merely a function of the additional washing procedure.

It has previously been suggested that under alkaline conditions, the dissociation of the O–H bond occurs in solution prior to adsorption onto the surface of the catalyst.[13] Scheme 2 illustrates how different surface mechanisms, which dictate the reaction selectivity, occur. Competitive dehydration and oxidation pathways proceed from GLD (**2.**). For the direct oxidation pathway, GLD binds to the surface of the catalyst and undergoes nucleophilic attack from $^{-}$OH, leading to the formation of a germinal diol surface intermediate. Subsequently, abstraction of the remaining hydrogen atom from the α-carbon by an additional $^{-}$OH anion leads to the formation of GLA (**3.**). The remaining primary alcohol in GA can subsequently undergo the same series of reactions, ultimately resulting in the formation of TA. Oxygen has an indirect role in this reaction. It has been demonstrated previously that the partial pressure of O_2 has no influence on the reaction selectivity and only influences the rate of glycerol consumption.[22] Davis and co-workers previously proposed that the role of O_2 in such systems is to serve as an electron scavenger; O_2 is reduced by H_2O in a parallel surface reaction.[13] This process consumes the electrons generated in dehydrogenation reactions, liberating actives sites and allowing additional substrate to interact with the surface. This explains why the rate of reaction under inert conditions is often

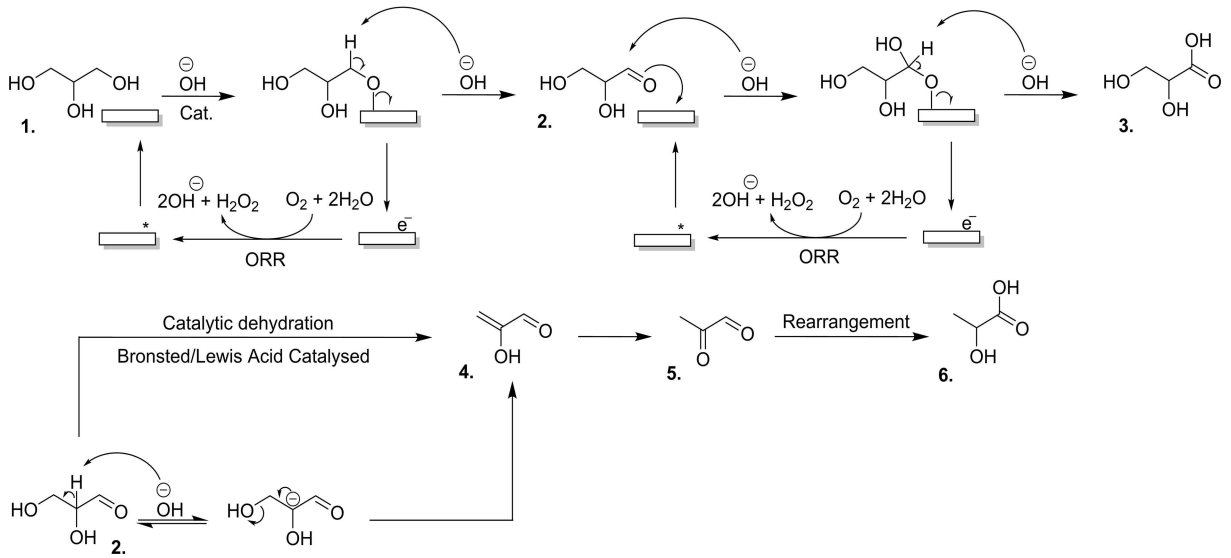

Scheme 2. Proposed reaction mechanism for the aerobic oxidation of glycerol over AuPt/TiO_2 catalysts under alkaline conditions. The mechanism provides insight into the competitive reaction pathways available; the direct oxidation pathway and the acidic and basic dehydration mechanisms. **Key:** 1. Glycerol; 2. Glyceraldehyde; 3. Glyceric acid; 4. 2-Hydroxyacrylaldehyde; 5. Pyruvaldehyde; 6. Lactic acid; * Active site vacancy; ORR – Oxygen reduction reaction.

© 2020 The Authors. Published by Wiley-VCH Verlag GmbH & Co. KGaA

significantly reduced and implies that oxygen incorporated into the acid products does not come from O_2 but ^{-}OH.

Competing with the formation of GA are three dehydration routes; a base promoted dehydration reaction, a Brønsted acid catalysed dehydration reaction, and Lewis acid catalysed dehydration reaction, which has been reported as being effective for this specific dehydration previously.[27] In the presence of NaOH, it is likely that many of the Bronsted acid sites would be neutralised. The result of this neutralisation is the exchange of the surface proton with a sodium cation, leading to the formation of a Lewis acid site and a molecule of water. Considering the dehydration reactions, we propose that the base catalysed dehydration is dominant. Given that this reaction occurs in solution and does not require interaction with the heterogeneous catalyst, it is understandable why reaction selectivity to LA increases with increasing NaOH concentration.[22] Each of these reactions lead to the formation of 2-hydroxyacrylaldehyde (**4.**), which undergoes a proton transfer to produce PALD (**5.**). From here, the PALD undergoes a base catalysed rearrangement to produce LA (**6.**).

As discussed previously, the presence of Si on the surface of the support clearly has a promotional effect on the formation of LA. We propose that the enhanced selectivity to LA over the AuPt/TiO_2–NC catalysts is a result of an increase in Brønsted acid sites on the surface of the catalyst. To establish whether this was indeed the case, NH_3–TPD experiments were conducted on the TiO_2–P25 and TiO_2–NC materials (Figure S3). A peak at *ca.* 500 °C was observed in the experiment over the NC material, which wasn't observed with the TiO_2–P25. This evidences a difference in the acidic sites present on the TiO_2–NC material. To further probe this phenomena, a series of *in situ* pyridine DRIFTS experiments were conducted on the TiO_2–P25, TiO_2–NC and TiO_2–NC–W supports. DRIFT spectra for the TiO_2–P25, TiO_2–NC and TiO_2–NC–W materials at 300 °C are displayed in Figure 5.

Different bands were observed in the 1350–1700 cm^{-1} range, corresponding to the ring modes of C–C and C–N. The frequency and sharpness of the strong absorbance appearing at 1445 cm^{-1} are associated with pyridine molecules chemisorbed at the Lewis acid sites (L–Py). The frequency of this mode is affected by the interaction between the pair of solitary nitrogen pyridine molecules and the Ti^{4+} ions at the substrate surface. The band at 1530 cm^{-1} identifies the formation of pyridinium ions (PyH^{+}) on the surface of the catalyst,[38,39] associated with Brønsted acid sites. Finally, the low-intensity band at 1490 cm^{-1} is due to the two contributions of both Brønsted and Lewis acid sites.[40,41] We can clearly observe in Figure 5, that whilst Lewis acid sites are detected in the TiO_2–P25, TiO_2–NC and TiO_2–NC–W materials, Brønsted acid sites are only apparent in the TiO_2–NC sample, and they are clearly removed after additional washing. Therefore, it can be tentatively proposed that Brønsted acid sites are formed on the support surface due to the interaction of TiO_2 and the remaining Si. The quantity of Brønsted and Lewis acid sites in each material was subsequently quantified from these spectra and the corresponding data are displayed in Table S5. The quantity of pyridine adsorbed on to Lewis and Brønsted acid sites decreases as the temperature

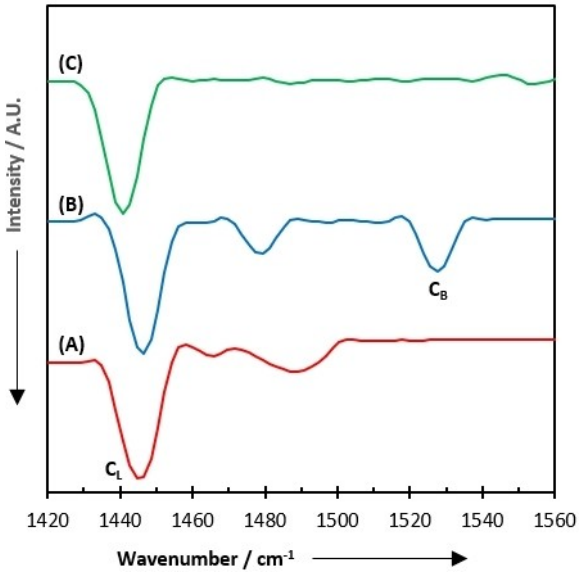

Figure 5. Pyridine DRIFT spectra for (A) TiO_2–P25, (B) TiO_2–NC and (C) TiO_2–NC–W.

increased from 50 °C to 400 °C. There is no evidence to suggest that the TiO_2–P25 and TiO_2–NC–W materials contain any Brønsted acid sites. There is however evidence to suggest that there is a substantial increase in the Lewis acidity in the TiO_2–NC material after the additional washing steps with NaOH, likely related to the presence of a higher amount of Ti^{4+} centres after Si removal.

We propose that these additional acid sites are indicative of a titanosilicate surface phase, formed from the inefficient etching of the silicon template. Indeed, a number of previous studies have confirmed that mixed metal oxides containing Si and Ti can consist of Brønsted acid sites.[42–44] Previous studies have confirmed that both Brønsted and Lewis acidic catalysts can catalyse the dehydration of a primary alcohol in this reaction.[26,27,45] This acid catalysed dehydration reaction also competes with the direct oxidation pathway, thereby providing an explanation to why higher reaction selectivity to LA is obtained in reactions over the AuPt/TiO_2–NC catalyst. Additional washing steps with aqueous NaOH led to the further removal of Si from the surface of the TiO_2–NC support (Figure 3 and Figure 4), and a resultant reduction in selectivity to LA (Table 2), was observed. This provides further evidence for the beneficial role of Si in the AuPt/TiO_2–NC catalyst. The co-operation of the two dehydration routes with the AuPt/TiO_2–NC catalyst is why higher selectivity to LA is obtained when compared to the AuPt/TiO_2–P25 catalyst. To further evidence this, additional experiments were conducted over the AuPt/TiO_2–NC and AuPt/TiO_2–P25 catalysts prepared by sol-immobilisation, with reduced equivalents of NaOH (Table S6). Interestingly, LA selectivity over of the NC supported catalyst appears to reduce as the pH of the system is lowered, suggesting that a co-operative effect between NaOH and the Si–NC exists. As such, we must conclude that the improvements in selectivity to

© 2020 The Authors. Published by Wiley-VCH Verlag GmbH & Co. KGaA

Table 3. High performing catalysts used for the aerobic oxidation of glycerol to LA, in the presence of NaOH. The corresponding reaction conditions and associated references are listed.

Catalyst	NaOH/Glycerol [mol/mol]	Temp. [°C]	Time [h]	O_2 pP [bar]	χ Glycerol [%]	LA selectivity [%]	Glycerol/metal ratio [mol/mol]	CMB [%]
$AuPt/TiO_2$[23]	4	90	–	1	30	86	–	99±3
$AuPt/TiO_2$[21]	2	60	2	4	80	50	114	95
Au/CeO_2[46]	4	90	–	0.2	98	83	–	94
$Au–Pt/nCeO_2$[22]	4	100	0.5	5	99	80	680	99–100
$Au–Pt/LaCrO_3$[24]	4	100	4	3	100	86	1000	–
$Pt_1Ni_1O_x/TiO_2$[47]	4	90	4	1	99	63	1000	–
Pt/C[48]	1.1	230	3	0.2	99	74	488	–
Pd/C[48]	1.1	230	3	0.2	99	68	266	–
Au_2Cu[49]	1.1	200	2	0.2	100	94	0	95
$AuPt/TiO_2–NC^{IMP}$	4	110	7	3	99	82	4055	102
$AuPt/TiO_2–NC^{SoL}$	4	110	7	3	100	71	4055	99

Key. Carbon mass balance (CMB); impregnation (IMP); sol-immobilisation (SOL); pP (partial pressure); χ (Conversion)

LA may not simply be a result of increased Bronsted and Lewis acidity in the TiO_2–NC supported catalyst.

The performance of the TiO_2–NC supported catalysts prepared by both sol- immobilisation and impregnation is competitive with other high performing catalysts already published in the literature (Table 3). They are evidently not the most selective towards LA, however, the high performance of these materials is justified when the relatively mild reaction conditions and comparatively low quantity of catalyst used in these experiments are considered. Furthermore, our studies have not concentrated on optimising catalyst performance, rather they have focused on developing understanding of the role of the support in the reaction. The observation that multiple dehydration pathways can function simultaneously, and the support properties have an influencing role, is the key observation here and will allow for further developments in catalyst design.

Conclusions

For glycerol selective oxidation a mesoporous nanocast TiO_2 support for AuPt nanoparticles led to enhanced selectivity to LA, compared to a $AuPt/TiO_2$–P25 catalyst. Reaction selectivity is controlled by the relative competitive rates of dehydration and oxidation reactions from GLD. The dehydration reaction predominantly occurs in solution and is catalysed by OH anions. However, residual quantities of Si remaining on the surface of the nanocast TiO_2 after etching resulted in the formation of Brønsted acid sites, which (i) may result in an additional Brønsted acid catalysed dehydration pathway and/or (ii) undergo dehydration to form Lewis acid sites in-situ due to the presence of NaOH, which can also promote the dehydration of primary alcohols. We propose that it is the combination of these two pathways which ultimately leads to increased reaction selectivity to LA with the nanocast $AuPt/TiO_2$ catalyst. Despite only modest enhancements in selectivity to LA being achieved herein, this work provides an enhanced understanding on the mechanistic involvement of the catalyst in this reaction and provides evidence that surface Brønsted/Lewis support acidity is an important characteristic that can be exploited to design more selective catalysts for this reaction.

Acknowledgments

T. García would like to acknowledge the Spanish MICINN through its Mobility program for stays of senior researchers and professors in foreign countries (grant number PRX18/00474) for funding. O.S.P acknowledges the FPI fellowship (BES-2016-077750) funded by Spanish MINECO. B.S. also thank MINECO (MAT2017-84118-C2-1-R project) for funding. We would also like to thank the Cardiff University TEM facility for the TEM and FEG-SEM electron microscopy data acquired and Diamond Light Source for access and support in use of the electron Physical Science Imaging Centre (Instrument E01 and proposal number MG21641 and MG22766) which contributed to the results presented here.

Conflict of Interest

The authors declare no conflict of interest.

Keywords: Aerobic Oxidation · Dehydration · Glycerol · Nanocasting · Lactic Acid.

[1] S. Veluturla, N. Archna, D. Subba Rao, N. Hezil, I. S. Indraja, S. Spoorthi, *Biofuels* **2018**, *9*, 305–314.
[2] R. A. Sheldon, *Green Chem.* **2014**, *16*, 950–963.
[3] Y. Wang, J. Zhou, X. Guo, *RSC Adv.* **2015**, *5*, 74611–74628.
[4] D. Sun, Y. Yamada, S. Sato, W. Ueda, *Appl. Catal. B* **2016**, *193*, 75–92.
[5] B. Katryniok, H. Kimura, E. Skrzyńska, J. S. Girardon, P. Fongarland, M. Capron, R. Ducoulombier, N. Mimura, S. Paul, F. Dumeignil, *Green Chem.* **2011**, *13*, 1960–1979.
[6] A. Villa, N. Dimitratos, C. E. Chan-Thaw, C. Hammond, L. Prati, G. J. Hutchings, *Acc. Chem. Res.* **2015**, *48*, 1403–1412.
[7] L. Prati, M. Rossi, *J. Catal.* **1998**, *176*, 552–560.
[8] L. Prati, G. Martra, *Gold Bull.* **1999**, *32*, 96–101.
[9] W. C. Ketchie, M. Murayama, R. J. Davis, *J. Catal.* **2007**, *250*, 264–273.
[10] A. Villa, D. Wang, G. M. Veith, L. Prati, *J. Catal.* **2012**, *292*, 73–80.

© 2020 The Authors. Published by Wiley-VCH Verlag GmbH & Co. KGaA

[11] S. A. Kondrat, P. J. Miedziak, M. Douthwaite, G. L. Brett, T. E. Davies, D. J. Morgan, J. K. Edwards, D. W. Knight, C. J. Kiely, S. H. Taylor, G. J. Hutchings, *ChemSusChem* **2014**, *7*, 1326–1334.
[12] J. Xu, H. Zhang, Y. Zhao, B. Yu, S. Chen, Y. Li, L. Hao, Z. Liu, *Green Chem.* **2013**, *15*, 1520–1525.
[13] B. N. Zope, D. D. Hibbitts, M. Neurock, R. J. Davis, *Science* **2010**, *330*, 74–78.
[14] N. Dimitratos, J. A. Lopez-Sanchez, D. Lennon, F. Porta, L. Prati, A. Villa, *Catal. Lett.* **2006**, *108*, 147–153.
[15] A. Villa, S. Campisi, K. M. H. Mohammed, N. Dimitratos, F. Vindigni, M. Manzoli, W. Jones, M. Bowker, G. J. Hutchings, L. Prati, *Catal. Sci. Technol.* **2015**, *5*, 1126–1132.
[16] W. C. Ketchie, Y. L. Fang, M. S. Wong, M. Murayama, R. J. Davis, *J. Catal.* **2007**, *250*, 94–101.
[17] A. Villa, G. M. Veith, D. Ferri, A. Weidenkaff, K. A. Perry, S. Campisi, L. Prati, *Catal. Sci. Technol.* **2013**, *3*, 394–399.
[18] S. A. Zavrazhnov, A. L. Esipovich, S. M. Danov, S. Y. Zlobin, A. S. Belousov, *Kinet. Catal.* **2018**, *59*, 459–471.
[19] M. R. A. Arcanjo, I. J. da Silva, C. L. Cavalcante, J. Iglesias, G. Morales, M. Paniagua, J. A. Melero, R. S. Vieira, *Biofuels, Bioprod. Biorefining* **2019**, *n/a*, bbb.2055.
[20] T. Komanoya, A. Suzuki, K. Nakajima, M. Kitano, K. Kamata, M. Hara, *ChemCatChem* **2016**, *8*, 1094–1099.
[21] E. A. Redina, O. A. Kirichenko, A. A. Greish, A. V. Kucherov, O. P. Tkachenko, G. I. Kapustin, I. V. Mishin, L. M. Kustov, *Catal. Today* **2015**, *246*, 216–231.
[22] R. K. P. Purushothaman, J. van Haveren, D. S. van Es, I. Melián-Cabrera, J. D. Meeldijk, H. J. Heeres, *Appl. Catal. B* **2014**, *147*, 92–100.
[23] Y. Shen, S. Zhang, H. Li, Y. Ren, H. Liu, *Chem. Eur. J.* **2010**, *16*, 7368–7371.
[24] C. D. Evans, S. A. Kondrat, P. J. Smith, T. D. Manning, P. J. Miedziak, G. L. Brett, R. D. Armstrong, J. K. Bartley, S. H. Taylor, M. J. Rosseinsky, G. J. Hutchings, *Faraday Discuss.* **2016**, *188*, 427–450.
[25] M. Tao, D. Zhang, X. Deng, X. Li, J. Shi, X. Wang, *Chem. Commun.* **2016**, *52*, 3332–3335.
[26] M. Tao, D. Zhang, H. Guan, G. Huang, X. Wang, *Sci. Rep.* **2016**, *6*, DOI 10.1038/srep29840.
[27] K. M. A. Santos, E. M. Albuquerque, G. Innocenti, L. E. P. Borges, C. Sievers, M. A. Fraga, *ChemCatChem* **2019**, *11*, 3054–3063.
[28] S. Feng, K. Takahashi, H. Miura, T. Shishido, *Fuel Process. Technol.* **2020**, *197*, 106202.
[29] H. J. Cho, C. C. Chang, W. Fan, *Green Chem.* **2014**, *16*, 3428–3433.
[30] Z. Tang, S. L. Fiorilli, H. J. Heeres, P. P. Pescarmona, *ACS Sustainable Chem. Eng.* **2018**, *6*, 10923–10933.
[31] D. Zhao, J. Feng, Q. Huo, N. Melosh, G. H. Fredrickson, B. F. Chmelka, G. D. Stucky, *Science* **1998**, *279*, 548–552.
[32] Y. Wang, B. Li, C. Zhang, L. Cui, S. Kang, X. Li, L. Zhou, *Appl. Catal. B* **2013**, *130–131*, 277–284.
[33] T. Barzetti, E. Selli, D. Moscotti, L. Forni, *J. Chem. Soc. Faraday Trans.* **1996**, *92*, 1401–1407.
[34] N. Pal, A. Bhaumik, *RSC Adv.* **2015**, *5*, 24363–24391.
[35] T. Ohno, K. Sarukawa, K. Tokieda, M. Matsumura, *J. Catal.* **2001**, *203*, 82–86.
[36] S. Cao, F. F. Tao, Y. Tang, Y. Li, J. Yu, *Chem. Soc. Rev.* **2016**, *45*, 4747–4765.
[37] A. Villa, D. Wang, G. M. Veith, F. Vindigni, L. Prati, *Catal. Sci. Technol.* **2013**, *3*, 3036–3041.
[38] F. Hemmann, I. Agirrezabal-Telleria, C. Jaeger, E. Kemnitz, *RSC Adv.* **2015**, *5*, 89659–89668.
[39] L. F. Isernia, *Mater. Res.* **2013**, *16*, 792–802.
[40] B. J. Lee, Y. G. Hur, D. H. Kim, S. H. Lee, K. Y. Lee, *Fuel* **2019**, *253*, 449–459.
[41] A. Platon, W. J. Thomson, in *Ind. Eng. Chem. Res.*, **2003**, pp. 5988–5992.
[42] Z. Liu, J. Tabora, R. J. Davis, *J. Catal.* **1994**, *149*, 117–126.
[43] T. Kataoka, J. A. Dumesic, *J. Catal.* **1988**, *112*, 66–79.
[44] X. Gao, I. E. Wachs, *Catal. Today* **1999**, *51*, 233–254.
[45] S. Lux, M. Siebenhofer, *Chem. Biochem. Eng. Q.* **2015**, *29*, 575–585.
[46] P. Lakshmanan, P. P. Upare, N. T. Le, Y. K. Hwang, D. W. Hwang, U. H. Lee, H. R. Kim, J. S. Chang, *Appl. Catal. A* **2013**, *468*, 260–268.
[47] Y. Li, S. Chen, J. Xu, H. Zhang, Y. Zhao, Y. Wang, Z. Liu, *Clean Soil Air Water* **2014**, *42*, 1140–1144.
[48] M. R. A. Arcanjo, I. J. Silva, E. Rodríguez-Castellón, A. Infantes-Molina, R. S. Vieira, *Catal. Today* **2017**, *279*, 317–326.
[49] L. Shen, X. Zhou, A. Wang, H. Yin, H. Yin, W. Cui, *RSC Adv.* **2017**, *7*, 30725–30739.

Manuscript received: January 6, 2020
Revised manuscript received: March 26, 2020
Version of record online: [redacted], [redacted]

© 2020 The Authors. Published by Wiley-VCH Verlag GmbH & Co. KGaA

FULL PAPERS

Synopses Nanocasting: Co-operation between Brønsted and Lewis acid sites and NaOH may lead to improved reaction selectivity for the aerobic oxidation of glycerol to lactic acid over AuPt supported catalysts under alkaline conditions. The physicochemical properties of the catalyst can influence the relative rates of glyceraldehyde oxidation and dehydration.

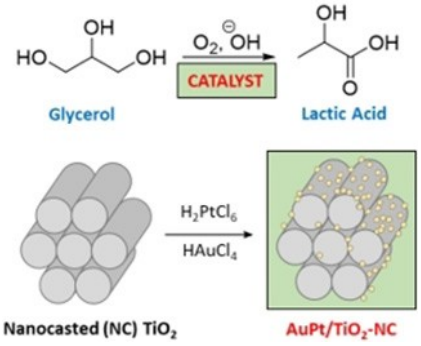

Dr. M. Douthwaite, N. Powell, A. Taylor, G. Ford, Dr. J. M. López, Dr. B. Solsona, Dr. N. Yang, O. Sanahuja-Parejo, Dr. Q. He, Dr. D. J. Morgan, Dr. T. Garcia, Prof. S. H. Taylor**

1 – 12

Glycerol Selective Oxidation to Lactic Acid over AuPt Nanoparticles; Enhancing Reaction Selectivity and Understanding by Support Modification